Journal of Power Sources 189 (2009) 248–255

Contents lists available at ScienceDirect

Journal of Power Sources

journal homepage: www.elsevier.com/locate/jpowsour

A comparative study of electrodes comprising nanometric and submicron particles of $LiNi_{0.50}Mn_{0.50}O_2$, $LiNi_{0.33}Mn_{0.33}Co_{0.33}O_2$, and $LiNi_{0.40}Mn_{0.40}Co_{0.20}O_2$ layered compounds

Surendra K. Martha[a], Hadar Sclar[a], Zvi Szmuk Framowitz[a], Daniela Kovacheva[b], Nikolay Saliyski[b], Yosef Gofer[a], Pessia Sharon[a], Eran Golik[c], Boris Markovsky[a], Doron Aurbach[a,*]

[a] Department of Chemistry, Bar-Ilan University, Ramat-Gan 52900, Israel
[b] Institute of General and Inorganic Chemistry, Bulgarian Academy of Sciences, Sofia 1113, Bulgaria
[c] Dr. Golik Chemical Instrumentation, Tel Aviv 66550, Israel

ARTICLE INFO

Article history:
Received 30 July 2008
Received in revised form 1 September 2008
Accepted 15 September 2008
Available online 2 October 2008

Keywords:
Li-batteries
Lithiated Mn–Ni–Co oxides
Cycling behavior
Rate capabilities
Surface reactions

ABSTRACT

In this paper we compare the behavior of $LiNi_{0.5}Mn_{0.5}O_2$, $LiNi_{0.33}Mn_{0.33}Co_{0.33}O_2$ (NMC) and $LiNi_{0.4}Mn_{0.4}Co_{0.2}O_2$ as cathode materials for advanced rechargeable Li-ion batteries. These materials were prepared by a self-combustion reaction (SCR) from the metal nitrates and sucrose, followed by calcination at elevated temperatures. The temperature and duration of calcination enabled the adjustment of the average particle size and size distribution. It was established that the annealing temperature (700–900 °C) of the as-prepared oxides influences strongly the crystallite and particle size, the morphology of the material, and the electrochemical performance of electrodes in Li-cells. Capacities up to 190, 180 and 170 mAh g^{-1} could be obtained with $Li[NiMn]O_2$, $LiNi_{0.4}Mn_{0.4}Co_{0.2}O_2$ and $LiNi_{0.33}Mn_{0.33}Co_{0.33}O_2$, respectively. In terms of rate capability, the order of these electrodes is NMC < $LiNi_{0.4}Mn_{0.4}Co_{0.2}O_2 \ll Li[NiMn]O_2$. Many hundreds of cycles at full DOD could be obtained with $Li[NiMn]O_2$ and NMC electrodes in Li-cells, at room temperature. All of these materials develop a unique surface chemistry that leads to their passivation and stabilization in standard electrolyte solutions (alkyl carbonates/$LiPF_6$). The surface chemistry was studied by FTIR, XPS and Raman spectroscopy and is discussed herein.

1. Introduction

In recent years, there is a growing interest in the layered compounds from the mixed Li–Ni–Mn–Co–O oxides family as materials for positive electrodes in Li-ion cells, due to their promising electrochemical and safety characteristics [1–4]. For instance, $LiNi_{0.5}Mn_{0.5}O_2$ electrodes may exhibit redox activity in the range of 3.0–4.6 V due to the presence of the redox couples Ni^{2+}/Ni^{4+} and Mn^{3+}/Mn^{4+}, which are responsible for higher capacity, and apparently better chemical stability compared to $LiCoO_2$ electrodes [5,6]. It was shown by Ohzuku et al. [7,8] that $Li/LiNi_{0.5}Mn_{0.5}O_2$ cells demonstrated about 200 mAh g^{-1} reversible capacity and stable performance at room temperature in the 2.5–4.5 V potential range during several dozens of cycles. Lithium–manganese oxides doped with other transition metals (cobalt or chromium) as materials for cathodes in lithium batteries have also been reported by several groups [9,10]. For instance, $LiNi_{1/3}Mn_{1/3}Co_{1/3}O_2$ electrodes have attracted much attention and many papers from different groups have appeared in the literature in recent year reporting on this cathode material [11]. It was found that these electrodes can operate in the voltage range of 2.5–4.6 V possessing sufficient structural and thermal stability, good cycle life, and delivering reversible capacity around 160–180 mAh g^{-1}. Several synthetic procedures have been proposed so far to produce lithiated oxide materials for cathodes of lithium batteries. For instance, it was demonstrated [12] that $LiNi_{1/3}Mn_{1/3}Co_{1/3}O_2$ materials prepared by the spray dry method and the metal acetate decomposition method differ in their morphology, particle size and shape. Hence, the electrochemical behavior of lithiated oxide electrodes may strongly depend on the synthetic methods of preparation [13]. Among them, combustion synthesis was used by Julien et al. [14] to prepare substituted lithium cobaltates $LiCo_{0.5}M_{0.5}O_2$ (M = Ni, Mg, Mn, Zn). They utilized respective aqueous solutions of metal nitrates as oxidants and urea as reducing agent in a combustion reaction, and the as-prepared oxides were calcined at 700 °C.

By studying lithium deintercalation mechanism from $Li_{1-y}Ni_{1/3}Mn_{1/3}Co_{1/3}O_2$ electrodes, Kobayashi et al. established [15] that the extraction of lithium ions from the structure proceeds mainly by the

* Corresponding author. Tel.: +972 3 531 8317; fax: +972 3 738 4053.
E-mail address: aurbach@mail.biu.ac.il (D. Aurbach).

0378-7753/$ – see front matter © 2008 Elsevier B.V. All rights reserved.
doi:10.1016/j.jpowsour.2008.09.090

oxidation processes of divalent nickel $Ni^{2+}/Ni^{3+}/Ni^{4+}$ and trivalent cobalt Co^{3+}/Co^{4+}. One of the major drawbacks of these electrodes is their low electronic conductivity [16]. We have shown in previous papers [17,18] that electrodes comprising nano-sized particles of lithiated oxides demonstrate a faster electrochemical kinetics, much higher capacity retention at high cycling rates, and lower impedance comparing to electrodes prepared from micrometric particles.

In the present work, we used self-combustion reaction (SCR) for the synthesis of nano-sized $LiNi_{0.5}Mn_{0.5}O_2$, $LiNi_{0.33}Mn_{0.33}Co_{0.33}O_2$ and $LiNi_{0.40}Mn_{0.40}Co_{0.20}O_2$ layered materials. It was shown that the particle size of the as-prepared lithiated oxides (30–50 nm) can be regulated by calcination (annealing) at 700–900 °C thus producing submicron particles of 0.2–0.5 μm. The above materials at different particle size were characterized and studied as active mass in cathodes for Li-cells in terms of electrodes' cycleability and rate capability. We studied also the surface chemistry aspects (by FTIR, Raman and photoelectron spectroscopy) related to $LiNi_{0.33}Mn_{0.33}Co_{0.33}O_2$ electrodes during their charge–discharge cycling and aging in standard alkyl carbonates/$LiPF_6$ solutions.

2. Experimental

Nanocrystalline $LiNi_{0.5}Mn_{0.5}O_2$, $LiNi_{0.33}Mn_{0.33}Co_{0.33}O_2$ and $LiNi_{0.40}Mn_{0.40}Co_{0.20}O_2$ layered materials were synthesized by the self-combustion method, from the stoichiometric amounts of lithium, nickel, manganese and cobalt nitrates, which act as the oxidants, and sucrose as the fuel. Typically, the reaction can be described as follows:

$$LiNO_3 + 0.5Ni(NO_3)_2{\cdot}6H_2O + 0.5Mn(NO_3)_2{\cdot}4H_2O + 0.3125C_{12}H_{22}O_{11} + 0.25O_2 \rightarrow LiNi_{0.5}Mn_{0.5}O_2 + 3.75CO_2 + 8.4375H_2O + 1.5\,N_2$$

The amount of sucrose used was chosen for the oxidant/fuel ratio = 1:1 [17,18]. In order to improve the crystallinity and to increase the crystallite size of the as-prepared samples they were then calcined (annealed) at 700 °C for 22 h and at 900 °C for 22 h, in air. The active surface areas of the above materials were measured by Brunauer, Emmet and Teller (BET) method with Gemini 2375, Micromeritics (multipoint mode). Their particle size was estimated from HRSEM images and particle size distribution was measured using Mastersizer-2000 (Malvern Instruments Ltd.). For instance, for the $LiNi_{0.40}Mn_{0.40}Co_{0.20}O_2$ material calcined at 900 °C/22 h the particle size distribution was found to be as follows: d(0.1) 0.228 μm, d(0.5) 0.335 μm, d(0.9) 0.628 μm. X-ray diffraction (XRD) measurements were performed using an AXS D8 Advance diffractometer (reflection θ–θ geometry, Cu Kα radiation, receiving slit 0.2 mm, scintillation counter, 40 mA, 40 kV) from Bruker, Inc. (Germany). The fitting of the XRD patterns was performed with the TOPAS-3 program, which is a part of the Bruker software package for structural analysis. HR-SEM images of the lithiated oxide particles were obtained by JEOL-JEM-2011 (200 kV) scanning electron microscope equipped with an Energy Dispersive X-ray Microanalysis System from Oxford Instruments. FTIR measurements of pristine and aged $Li[MnNiCo]O_2$ powders were carried out using diffuse reflectance mode (accessory from Pike Technologies Inc.) with a Nicolet Magna 560 FTIR spectrometer, placed in a glove box, under H_2O and CO_2 free atmosphere (air purifier from Balston Inc.). X-ray photoelectron spectroscopy (XPS) measurements were carried out using HX Axis systems from Kratos, Inc. with monochromic AlKα (1486.6 eV) X-ray beam radiation, binding energy was calibrated *vs.* carbon (C1s = 285 eV). For these measurements, the powder samples were transferred to the XPS device using a home made hermetically sealed unit, which contains a sample holder attached to a magnetic manipulator, and a gate valve. Chemical analysis of the solutions remaining after aging of cathode materials was carried out using ICP spectrometer Ultima-2 (Jobin Yvon Horiba). In order to remove organics from these solutions, we used the following procedure: 1 mL of H_2SO_4:HNO_3 (1:1) was added to 0.2 mL of the remaining solution and kept overnight at room temperature in a sealed Teflon vial. Afterwards, the volume of the mixture was adjusted to 25 mL by adding double-distilled water (DDW) and it was heated on a sand-bath at 110 °C for several hours. The volume of the mixture was finally adjusted by DDW to 10 mL.

Electrochemical measurements were conducted in two- and three-electrode coin-type cells (standard parts, model 2325 NRC, Canada) or in pouch cells (aluminum coated polypropylene) with a polypropylene membrane separator (Celgard, Inc.). The working composite electrodes comprised 80% (by weight) of the active lithiated oxide material, 10% super P carbon black and 10% PVdF binder, prepared as a slurry in N-methyl-pyrollidone that was pasted on both sides of Al-foil current collectors (>99.9%, Strem Chemicals Inc., USA). The working electrodes active mass was usually 2–4 mg for coin-cells and 25–40 mg for pouch cells. We also prepared binder and carbon-free electrodes, comprising the lithiated oxide powders embedded by pressure onto the Al current collectors, as described elsewhere [17,18]. There electrodes were very suitable for spectroscopic measurements, in which only the response of the active mass was studied with no interference by side reactions of the polymeric binder and the high surface area carbon black additive with solution species. All the potentials in this work are given *vs.* Li/Li^+ reference electrodes. Electrochemical cells were assembled in glove boxes filled with highly pure argon (VAC, Inc.). The electrolyte solutions comprising dimethyl carbonate (DMC) and ethylene carbonate (EC) (2:1, by weight) and 1.5 M $LiPF_6$ were obtained from Tomiyama, as Li battery grade and could be used as received. The content of HF and H_2O in solution was around 100 and 20 ppm, respectively. After assembling, electrochemical cells were stored at room temperature for 12–24 h to ensure complete impregnation of the electrodes and separators with the electrolyte solutions. The electrochemical measurements were carried out using a battery test unit model 1470 coupled with a FRA model 1255 from Solartron, Inc. (driven by the Corrware and ZPlot software from Scribner Associates), and a multichannel battery test unit from Maccor, Inc., model 2000. Two-electrode cells were tested in the potential range of 2.5–4.5 V using constant current–constant voltage (CC–CV) protocol at various rates with a potentiostatic step at the cut-off potential. The duration of the potentiostatic (charging) steps was adjusted to the currents applied at the galvanostatic charging steps and they varied from 5 h for C/10 rates to 10 min for 3C rates. The accuracy of the calculations of electrodes' capacity in all the graphs presented herein is around ±5%. Aging of $Li[MnNiCo]O_2$ particles in DMC–EC/$LiPF_6$ solutions (magnetic stirring) was carried out in a glove box at 30 °C.

3. Results and discussion

Fig. 1 shows XRD patterns of the $LiNi_{0.5}Mn_{0.5}O_2$, $LiNi_{0.33}Mn_{0.33}Co_{0.33}O_2$ and $LiNi_{0.40}Mn_{0.40}Co_{0.20}O_2$ layered materials (powders) produced by SCR, which were further annealed at 900 °C during 22 h in air. The diffraction lines in this figure can be indexed on the basis of a hexagonal lattice structure of α-$NaFeO_2$, space group 166, $R\bar{3}m$. We conclude from these XRD results that there are no remarkable impurities in the materials thus obtained. Minor peaks at 2θ around 21–22° in the XRD pattern of some of the $LiNi_{0.5}Mn_{0.5}O_2$ samples, may indicate the presence (a few weight

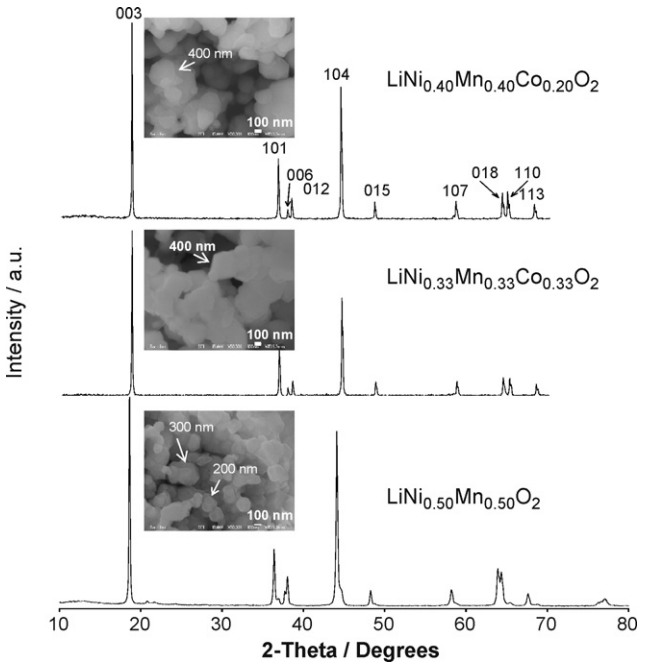

Fig. 1. XRD patterns of the $LiNi_{0.5}Mn_{0.5}O_2$, $LiNi_{0.33}Mn_{0.33}Co_{0.33}O_2$ and $LiNi_{0.40}Mn_{0.40}Co_{0.20}O_2$ particles obtained by self-combustion reactions and annealed further in air at 900 °C for 22 h. Miller indexes of main reflections are indicated. Insets are HRSEM images of the above particles (50,000×, scale bars are 100 nm).

%) of a secondary phase ($LiNiO_2$). Highly resolved splitting of the 0 0 6/0 1 2 and 0 1 8/1 1 0 peaks of the $LiNi_{0.33}Mn_{0.33}Co_{0.33}O_2$ and $LiNi_{0.40}Mn_{0.40}Co_{0.20}O_2$ materials and the ratio of the lattice parameters c/a = 4.96–4.98 provide evidence of a characteristic well-ordered layered structure of these compounds. Moreover, the ratios of the integrated intensities of the 0 0 3 and the 1 0 4 peaks in the XRD patterns, were found to be around 1.2 and >1, respectively for the above materials. This may indicate therefore no pronounced cation mixing [19] and thereby the electrochemical activity of these cathode materials in terms of capacity and rates of Li deinsertion/insertion is supposed to be very good (comparable to results presented by Makimura and Ohzuku [7]). The low values of the *R*-factor $R = (I_{102} + I_{006})/I_{101}$, around 0.41–0.44, which relates to the integrated intensities of the corresponding well-resolved peaks of the $LiNi_{0.33}Mn_{0.33}Co_{0.33}O_2$ and $LiNi_{0.40}Mn_{0.40}Co_{0.20}O_2$ materials also confirm their high hexagonal ordering [20,21].

The insets in Fig. 1 show HRSEM images of the $LiNi_{0.5}Mn_{0.5}O_2$, $LiNi_{0.33}Mn_{0.33}Co_{0.33}O_2$ and the $LiNi_{0.40}Mn_{0.40}Co_{0.20}O_2$ particles prepared by calcinations at 900 °C for 22 h. All of these particles are of submicron size, between 0.1 and 0.5 μm. The $LiNi_{0.5}Mn_{0.5}O_2$ particles have mostly hexagonal shape while those of $LiNi_{0.33}Mn_{0.33}Co_{0.33}O_2$ and $LiNi_{0.40}Mn_{0.40}Co_{0.20}O_2$ are of irregular shape and have plate-like morphology. Individual $LiNi_{0.5}Mn_{0.5}O_2$ particles obtained by calcination at 700 °C for 22 h have nano-sized dimensions of 60–75 nm. We have found that annealing at higher temperature (900 °C) leads to increasing the particle size up to submicron (around 0.2 μm). Similarly, rising the calcination temperature of the $LiNi_{0.33}Mn_{0.33}Co_{0.33}O_2$ and $LiNi_{0.40}Mn_{0.40}Co_{0.20}O_2$ compounds result in growing particle size from nanometric to submicron (0.2–0.5 μm).

From the element analysis by ICP and by energy dispersive spectroscopy (EDS, measured during imaging by SEM) Mn/Ni atomic ratio of 1:1 was measured for $LiNi_{0.5}Mn_{0.5}O_2$ powders and Mn/Ni/Co atomic ratios of 1:1:1 and 1:1:0.5 (±5%) were measured for the $LiNi_{0.33}Mn_{0.33}Co_{0.33}O_2$ and the $LiNi_{0.40}Mn_{0.40}Co_{0.20}O_2$ compounds synthesized in this work, respectively. Lattice parameters, crystallite size calculated from the Scherrer's equation, particle size estimated from the HRSEM images, surface area (N_2 adsorption BET model), ratios of the intensities of the main 0 0 3 and 1 0 4 XRD peaks, and values of the *R*-factor of all the lithiated transition metal oxides synthesized herein, are summarized in Table 1.

As expected, crystallite and particle size increase substantially with increasing the calcination temperature, however the conditions of annealing influence slightly the lattice parameters. Specific surface area of these materials decreases significantly if the calcination temperature increases from 700 to 900 °C. This allowed us to follow the electrochemical performance of the cathodes comprising nano-sized or submicron particles of the $LiNi_{0.5}Mn_{0.5}O_2$, $LiNi_{0.33}Mn_{0.33}Co_{0.33}O_2$ and $LiNi_{0.40}Mn_{0.40}Co_{0.20}O_2$ layered materials with various active areas.

Fig. 2a shows data on representative rate capability (discharge capacity *vs.* cycle number at different C rates as indicated) of electrodes comprising nano-$LiNi_{0.5}Mn_{0.5}O_2$ particles (70 nm, calcination at 700 °C/22 h). The inset in this figure compares slow scan rate CVs (50 μV s^{-1}) of electrodes comprising nano- and submicron size particles. Examining qualitatively these CVs, they reflect the faster kinetics of the nano-material: sharper redox peaks and smaller peaks separation. Fig. 2b and c shows similar data: capacity *vs.* discharge rate in experiments which involved prolonged cycling, for $LiNi_{0.5}Mn_{0.5}O_2$ and $LiNi_{0.33}Mn_{0.33}Co_{0.33}O_2$ electrodes, comprising submicron particles (around 0.2–0.45 μm, calcination at 900 °C/22 h). The typical cycle life that could be reached with these electrodes during hundreds of charge–discharge cycles at high rates is also demonstrated in Fig. 2b and c. Typically, nano-$LiNi_{0.5}Mn_{0.5}O_2$ electrodes (particle size around 70 nm) exhibit initial discharge capacity of 160 mAh g^{-1} at low rates, high capacity retention (98%) upon cycling these electrodes at various rates up to 3C (and back to low rates) and stable prolonged cycling behavior at various rates.

By comparing the results represented in Fig. 2a and b, it is found that electrodes comprising submicron particles of $LiNi_{0.5}Mn_{0.5}O_2$ (annealed at 900 °C/22 h) behave similarly to their nano-counterparts while they demonstrate higher discharge capacities at a wide range of rates (e.g., from C/5 to 3C rates, Fig. 2b). This may relate to higher crystallinity of the submicron particles

Table 1
Listing of crystallite size, particle size, specific surface area, lattice parameters, and ratios of the XRD peaks intensities for the various lithiated transition metal oxides synthesized in the framework of this work, as a function of their final annealing conditions (temperature/time).

Synthesized material	Conditions of annealing	Crystallite size (nm)	Particle size, nm (SEM)	Active area (m^2/g)	Lattice parameters			c/a	$\frac{I_{003}}{I_{104}}$	$R = \frac{I_{006}+I_{012}}{I_{101}}$
					a (Å)	c (Å)	Cell volume (Å)^3			
$LiNi_{0.50}Mn_{0.50}O_2$	700 °C/22 h	37	60–75	6.5	2.899	14.257	103.81	4.92	0.76	0.74
	900 °C/22 h	71	150–200	3.5	2.893	14.292	103.60	4.94	0.83	0.62
$LiNi_{0.33}Mn_{0.33}Co_{0.33}O_2$	700 °C/22 h	41	40–60	6.2	2.862	14.243	101.02	4.97	1.24	0.44
	900 °C/22 h	98	200–450	2.6	2.864	14.261	101.34	4.98	1.17	0.41
$LiNi_{0.40}Mn_{0.40}Co_{0.20}O_2$	700 °C/22 h	24	25–60	11.0	2.869	14.227	101.42	4.96	1.00	0.42
	900 °C/22 h	105	100–500	4.0	2.874	14.280	102.13	4.97	1.06	0.39

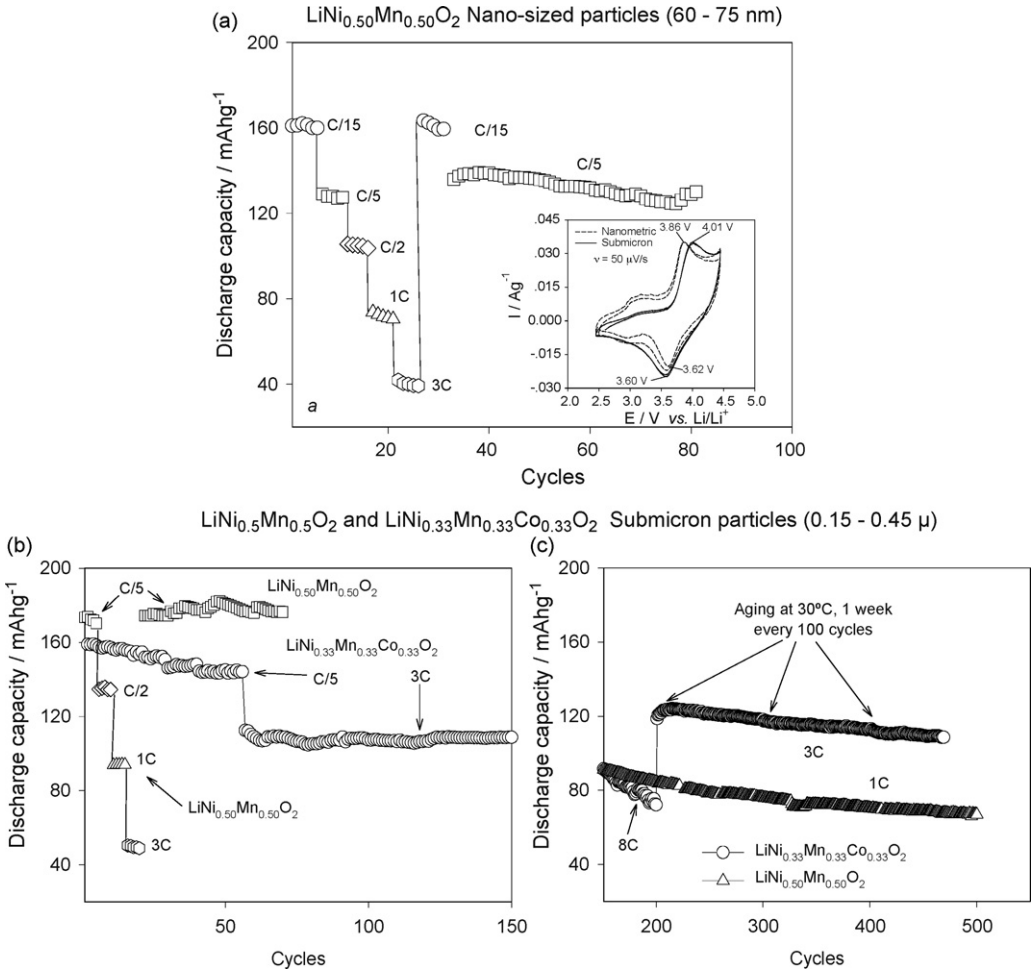

Fig. 2. (a) Cycling behavior at various rates of discharge (as indicated) of the composite electrode comprising nano-sized $LiNi_{0.5}Mn_{0.5}O_2$ particles produced by SCR and further annealed in air at 700 °C for 22 h. Coin-type cell, T = 30 °C, potential range was 2.5–4.5 V. Cycling protocol was constant current–constant voltage providing potentiostatic steps at 4.5 V during 5 h for C/15 and C/10 rates, 2.5 h for C/5 rates, 1 h for C/2 rates, 30 min for 1C rates and 10 min at 3C rates. The inset shows cyclic voltammograms (50 $\mu V\,s^{-1}$) measured from thin-layer electrodes comprising nanometric size $LiNi_{0.5}Mn_{0.5}O_2$ (annealing at 700 °C during 22 h) and submicron particles of the same material (annealing at 900 °C during 22 h). The electrodes were prepared by embedding $LiNi_{0.5}Mn_{0.5}O_2$ powder by pressure onto the Al-foil current collector and they were free of PVdF and carbon black. (b) Cycling behavior at various rates of discharge (as indicated) of electrodes comprising submicron $LiNi_{0.5}Mn_{0.5}O_2$ and $LiNi_{0.33}Mn_{0.33}Co_{0.33}O_2$ particles produced by SCR and further annealed in air at 900 °C during 22 h. Coin-type cells, T = 30 °C, potential range was 2.5–4.5 V. Cycling protocol was similar to that of Fig. 2a. (c) Prolonged cycling of the same $LiNi_{0.33}Mn_{0.33}Co_{0.33}O_2$ electrode, as in Fig. 2b. After 150 cycles at C/5 and 3C, this electrode was cycled additionally at 8C and subsequently at 3C with periodically aging the cell at discharged states during 1 week, every 100 cycles. For comparison, the typical dependence of the discharge capacity of electrodes comprising submicron $LiNi_{0.5}Mn_{0.5}O_2$ particles on the cycle number during prolonged galvanostatic cycling at 1C rates is also presented.

due to the elevated temperature of their annealing. In addition, nano-particles of this material are characterized by higher value of cation mixing and they have lower degree of hexagonal ordering, as follows from the structural analysis summarized in Table 1. Although the electrodes comprising nano-$LiNi_{0.5}Mn_{0.5}O_2$ particles demonstrate faster electrochemical kinetics in comparison to those prepared from submicron or micronic particles [17,18], it seems that the calcination conditions influence strongly the cation ordering/disordering, and therefore, the electrochemical activity of the material. Annealing at 700 °C for 22 h may be considered as inappropriate for obtaining $LiNi_{0.5}Mn_{0.5}O_2$ cathode material with desirable cycling properties. Typically, $LiNi_{0.5}Mn_{0.5}O_2$ cathodes comprising submicron particles display very stable cycling at 1C rate during more than 350 charge/discharge cycles (Fig. 2b and c). Capacity fading was found to be around 0.1 mAh g^{-1} per cycle in this case. As regarding $LiNi_{0.33}Mn_{0.33}Co_{0.33}O_2$ and $LiNi_{0.40}Mn_{0.40}Co_{0.20}O_2$ electrodes made from submicron particles, it is expected that these electrodes would demonstrate good electrochemical performance in terms of capacity rate capability and cycleability due to high hexagonal ordering (c/a values of 4.96–4.97), lesser exchange of Ni^{2+} and Li^+ cations in their (3a) and (3b) sites, respectively, as well as small values of the R-factor (Table 1). Indeed, $LiNi_{0.33}Mn_{0.33}Co_{0.33}O_2$ electrodes show remarkable highly stable performance at high rates (e.g., 3C–8C rates, namely full capacity within 20 min and less than 8 min of discharge, respectively) and cycling tests at various rates during hundreds of cycles at 30 °C, as seen from Fig. 2b and c. The capacity retention found with these electrodes was impressive even when these cycling experiments included prolonged aging. This may be attributed, to some extent, to small enough specific surface area (2.6 $m^2\,g^{-1}$) of the $LiNi_{0.33}Mn_{0.33}Co_{0.33}O_2$ submicron particles. By comparing $LiNi_{0.33}Mn_{0.33}Co_{0.33}O_2$ and $LiNi_{0.40}Mn_{0.40}Co_{0.20}O_2$ materials obtained by SCR and calcined at the same conditions, we see comparable crystallite and particle size and also little changes in the parameters deduced from the structural XRD analysis (Table 1). Fig. 3 demonstrates that $LiNi_{0.33}Mn_{0.33}Co_{0.33}O_2$ electrodes deliver higher discharge capacities (around 160–150 mAh g^{-1}) than that of the $LiNi_{0.40}Mn_{0.40}Co_{0.20}O_2$ cathodes (around 140–130 mAh g^{-1}) prepared from submicron particles, at similar discharge rates at 30 °C (Figs. 2b and c and 3). Typically, electrodes made from these

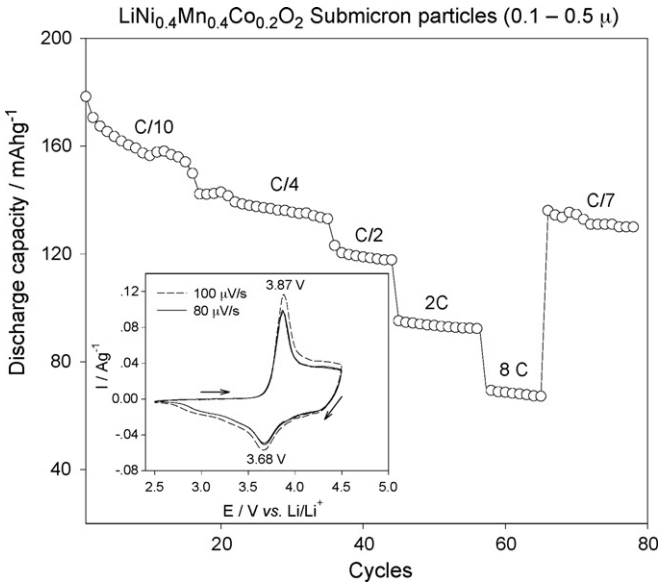

Fig. 3. Typical results of cycling tests (capacity as a function of rates) of electrodes comprising submicron $LiNi_{0.40}Mn_{0.40}Co_{0.20}O_2$ particles produced by SCR and further annealed in air at 900 °C during 22 h. Coin-type cell, T = 30 °C, potential range was 2.5–4.5 V. Cycling protocol was similar to that of Fig. 2a. The inset presents steady-state cyclic voltammograms measured with a $LiNi_{0.40}Mn_{0.40}Co_{0.20}O_2$ electrode (submicron particles), T = 30 °C, pouch cell, potential range: 2.5–4.5 V.

materials deliver comparable capacities of ca. 200–210 mAh g^{-1} in the first charge (delithiation) and ca. 170–180 mAh g^{-1} in the first discharge (lithiation) processes, respectively. However, it was established that $LiNi_{0.33}Mn_{0.33}Co_{0.33}O_2$ electrodes (submicron particles) seem to have higher reversible capacity, superior cycling and rate capability properties as discussed above. $LiNi_{0.40}Mn_{0.40}Co_{0.20}O_2$ electrodes prepared from submicron particles demonstrate fast enough electrochemical kinetics and reversibility at 30 °C, as also demonstrated (qualitatively) by steady-state CVs shown in the inset to Fig. 3. Work is in progress to compare electrochemical stability, capacity retention, rate capabilities, and voltammetric behavior of electrodes prepared from $LiNi_{0.5}Mn_{0.5}O_2$, $LiNi_{0.33}Mn_{0.33}Co_{0.33}O_2$ and $LiNi_{0.4}Mn_{0.4}Co_{0.2}O_2$ cathode materials at elevated temperatures (50–60 °C).

The surface chemistry of lithiated transition metal oxides used as cathode materials for Li-ion batteries was studied intensively by us during the past decade. We could identify several possible surface reactions of Li_xMO_y cathode material in electrolyte solutions based on alkyl carbonate solutions. The surface oxygen of these oxides can attack nucleophilically alkyl carbonate molecules, thus forming surface $ROCO_2Li$, $(ROCO_2)_yM$, ROLi and $(RO)_xM$ species [17,18,22,23].

The basic oxygen reacts with acidic species such as HF, thus forming surface fluorides (LiF, MF_x). Transition metals at high oxidation states can oxidize alkyl carbonates, thus forming CO_2 and transition metal ions at lower oxidation states. Such ions can dissolve in solutions more easily than transition metal ions at high oxidation states. The dissolution of transition metal ions changes the stoichiometry of the active mass [22]. Consequently, the surface structure of the transition metal oxides changes, thus forming core–shell type morphology [17,18]. Finally, alkyl carbonates, especially cyclic molecules such as EC, can be polymerized on the Li_xMO_y particles' surfaces, probably by cationic mechanisms, to form polycarbonate species. The order of reactivity of Li_xMO_y compounds in standard solutions based on alkyl carbonate solvents and $LiPF_6$ was found to be $LiNiO_2$ > $LiCoO_2$ > $LiMnO_2$ (layered) and $LiMn_2O_4$ spinel [23].

In recent years, we studied the performance and surface chemistry of $LiMn_{1.5}Ni_{0.5}O_4$ spinel and $LiMn_{0.5}Ni_{0.5}O_2$ layered compounds as cathode materials in composite electrodes for Li-ion batteries [18,24,25]. These materials were also found to be very reactive towards solution species in standard electrolyte solution based on alkyl carbonates and $LiPF_6$. These materials seem to develop surface films comprised of Li and transition metal fluorides, alkoxides and metal alkyl carbonate species, and polycarbonates. We found evidence that upon aging in solutions, the particles of these $Li[MnNi]O_2$ materials develop a core–shell structure. The shell is formed by the surface reactions and the reversible dissolution of transition metals that leads to changes in the stoichiometry of the material near the surface, and hence, to the formation of new phases.

In the present work, the surface chemical studies concentrated on $LiNi_{0.33}Mn_{0.33}Co_{0.33}O_2$ powder and electrodes.

Fig. 4 shows FTIR spectra measured by the diffuse reflectance from pristine and aged $LiNi_{0.33}Mn_{0.33}Co_{0.33}O_2$ powders. Aging was carried out in an EC–DMC 1:2/$LiPF_6$ 1.5 M solution in dynamic conditions (magnetic stirring) during 3 weeks at 30 °C. The amount of dissolved Ni, Mn, and Co from the lithiated oxide was around 0.002–0.01%, as detected by the ICP analysis. This solution was chosen because it was found to be one of the most appropriate for use with cathodes operating at high red-ox potentials (e.g., $LiMn_{1.5}Ni_{0.5}O_4$, up to 4.9 V *vs.* Li/Li^+) [18,24,25]. This is probably due to the optimal ratio between EC and DMC concentrations, higher content of the lithium salt and lesser amounts of contaminants (H_2O and HF). A typical solution spectrum is also included in Fig. 4, as indicated. The spectrum related to the pristine powder is nearly featureless in most of the relevant range. The main IR peaks are of the surface –OH groups (3360 cm^{-1}), residual atmospheric CO_2 (indicated) and peaks at low wavenumbers (400–600 cm^{-1}) that probably belong to M–O vibrations. The IR spectrum of the aged powder is rich in peaks, around 3000 cm^{-1} (related to C–H bonds), around 1800–1600 cm^{-1} (carbonyl C=O peaks), and many peaks below 1450 cm^{-1}, which belong to the fingerprint region of organic species. The comparison with solution spectrum shows that the spectrum of the aged electrode material does not reflect the presence of residual EC. Hence, the carbonyl peaks in the 1800–1600 cm^{-1} range in the spectrum of the aged $LiNi_{0.33}Mn_{0.33}Co_{0.33}O_2$ powder indeed reflect the formation of polycarbonate and $ROCO_2M$ species.

Fig. 5 compares XPS peaks of O1s, F1s and P2p measured from pristine and aged $LiNi_{0.33}Mn_{0.33}Co_{0.33}O_2$ powders. Aging included storage at 60 °C in an EC–DMC 1:2/1.5 M $LiPF_6$ solution. These surface studies demonstrate pronounced changes in the surface composition of this material upon contact with the electrolyte solutions. The fluorine and phosphorous peaks in the spectra obviously reflect surface species that were formed by reactions between the cathode material and solution species. The oxygen peaks also reflect pronounced surface changes. The new broad oxygen peak at high binding energies (up to 535 eV) reflects the formation of surface oxygen compounds with higher oxidation state compared to that of the oxygen atoms in the bulk metal oxide. This is in line with the FTIR spectrum of the aged material that reflects the formation of surface carbonate and polycarbonate species.

Fig. 6 presents XPS data related to the transition metals, Co, Mn and Ni (2P 2/3) of pristine, aged, and charged $LiNi_{0.33}Mn_{0.33}Co_{0.33}O_2$ electrodes in EC–DMC 1:2/$LiPF_6$ 1.5 M solutions at 60 °C. The charged electrode underwent a few cycles in the 2.5–4.5 V potential range before the measurements. The final potential that the charged electrode reaches before the XPS measurements was 4.3 V. As seen in Fig. 6, the XPS studies of these electrodes clearly show that upon aging in solutions, Ni remains on the surface, while Co and Mn either disappear from the surface or their concentration

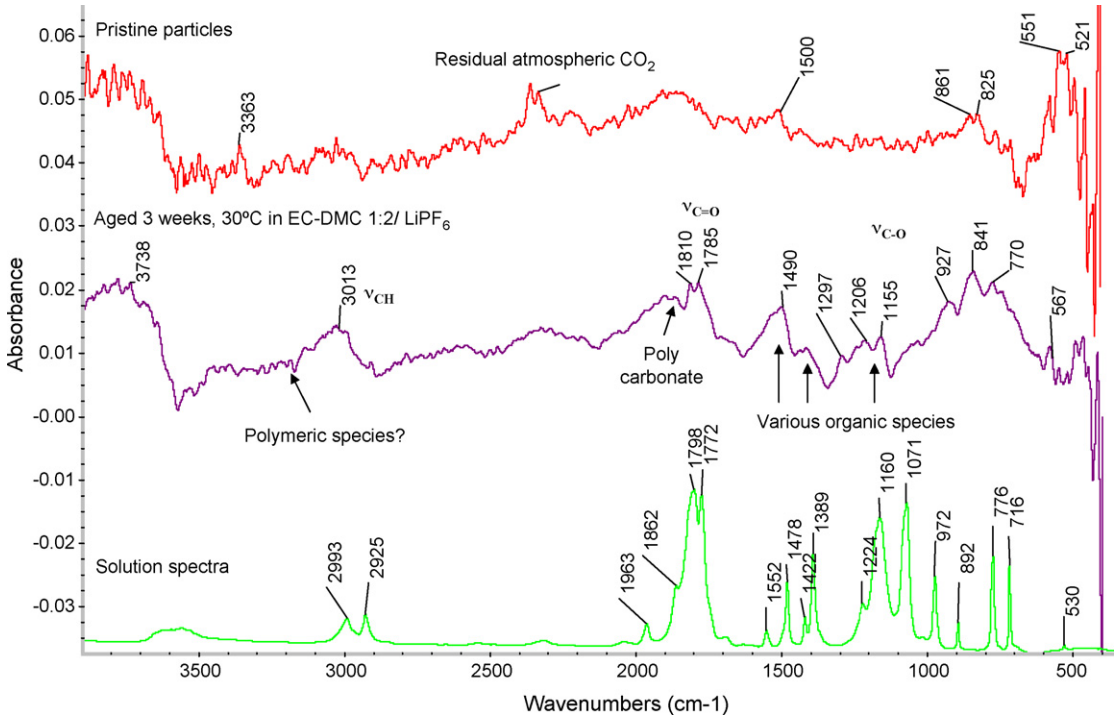

Fig. 4. FTIR spectrum of pristine $LiNi_{0.33}Mn_{0.33}Co_{0.33}O_2$ nano-particles (calcination at 700 °C/1 h after SCR) and spectrum of nano-particles aged in an EC–DMC/$LiPF_6$ solution, at 30 °C for 3 weeks. Aging in the above solution was carried out in the glove box using magnetic stirring. IR spectrum of the solution is also presented, as indicated, for comparison.

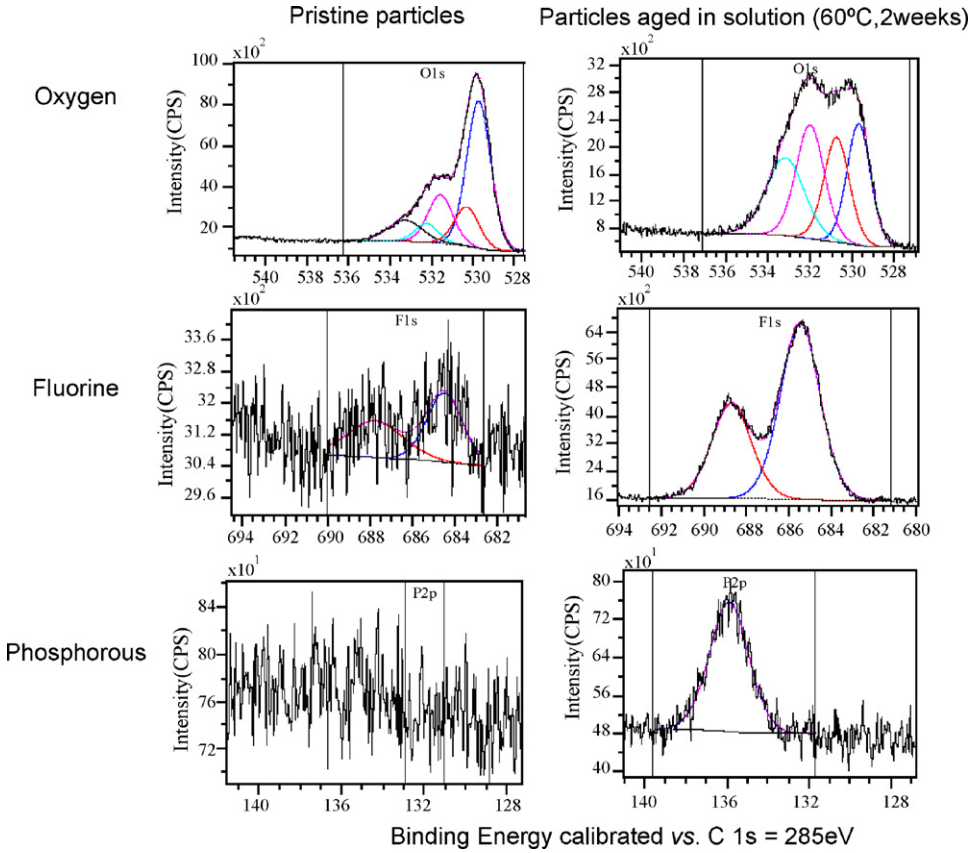

Fig. 5. XPS spectra (O1s, F1s and P2p) of pristine $LiNi_{0.33}Mn_{0.33}Co_{0.33}O_2$ nano-particles (calcination at 700 °C/1 h after SCR) and spectra of nano-particles aged in an EC–DMC/$LiPF_6$ solution, at 60 °C for 2 weeks.

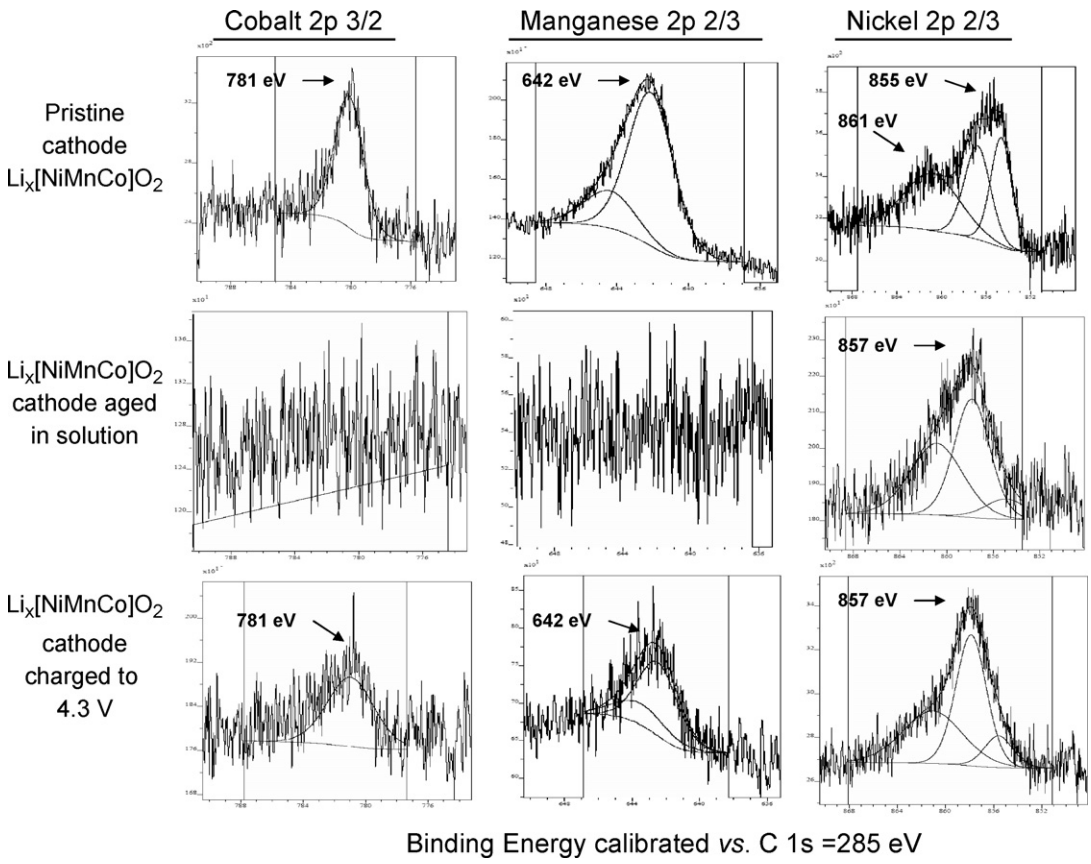

Fig. 6. XPS spectra (Ni, Mn, Co as indicated) of pristine electrode comprising $LiNi_{0.33}Mn_{0.33}Co_{0.33}O_2$ nano-particles (calcination at 700 °C/1 h after SCR), spectra of cycled and then charged to 4.3 V $LiNi_{0.33}Mn_{0.33}Co_{0.33}O_2$ electrode and spectra of aged $LiNi_{0.33}Mn_{0.33}Co_{0.33}O_2$ electrode in an EC–DMC/$LiPF_6$ solution (60 °C, 1 day). The electrodes for these tests were prepared by embedding $LiNi_{0.33}Mn_{0.33}Co_{0.33}O_2$ powder by pressure onto Al-foil current collectors and they were free of PVdF and carbon black.

diminishes, compared to the pristine material. We explored possible dissolution of transition metals from $LiNi_{0.33}Mn_{0.33}Co_{0.33}O_2$ powder into EC–DMC/$LiPF_6$ solutions (excess of solution, no saturation condition). It was found that the dissolution rate of Mn ions is twice than that of Ni and Co ions (same rates of dissolution for the latter ions). This finding means that the surface species formed on the active mass as indicated by the above-described spectral studies passivate the surface and prevent the continuous dissolution of the transition metal cations from the lithiated [NiMnCo] oxide. We can explain the spectral results presented in Fig. 6 in light of our previous studies that showed that $LiNiO_2$ is the most reactive cathode material compared to $LiCoO_2$ and $LiMn_2O_4$. We can speculate that the oxygen bound to Ni may be more nucleophilic and basic, compared to the oxygen bound to Co and Mn. Hence, the predominant reactions of Ni-bound oxygen with acidic and electrophilic solution species preferably form Ni-containing surface species such as NiF_x $(ROCO_2Li)_xNi$, $(RO)_xNi$, etc., which leave Ni on the particles' surface, but mask the bulk of the active mass that contains Mn and Co at the same concentrations as Ni.

The above description of the surface chemistry of Li[NiMnCo]O_2 is based on solid observation, but is still ambiguous in terms of the exact identification of the surface compounds thus formed, their relative quantities, and the depth profiling of the surface layers. However, this is the general nature of surface studies, i.e., it is much more ambiguous than bulk structural studies. The identification of thin films by surface sensitive techniques such as FTIR, XPS, Raman spectroscopy, and electron microscopy (with element analysis and electron diffraction) is indeed a difficult, and sometimes impossible, task.

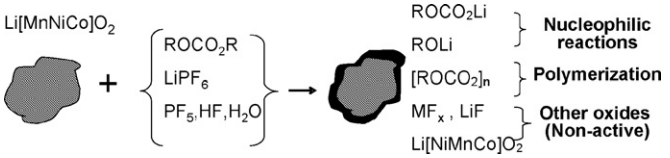

Fig. 7. A presentation of the formation of the core–shell structure of the Li[MnNiCo]O_2 particles formed due to their surface reactions in solutions.

Our main findings in the above-described surface studies are summarized in Fig. 7, which presents several surface reaction paths, their surface species products, and the resulting formation of particles with a core–shell structure.

4. Conclusions

Self-combustion reactions based on transition metal nitrates, Li nitrate and sucrose are versatile methods for producing layered Li[NiMn]O_2 and Li[NiMnCo]O_2 compounds with adjustable particle size. Using SCR, following by calcination in air, nano-, submicronic and micron size particles can be produced as a function of the temperature and duration of the final calcination process. $LiNi_{0.5}Mn_{0.5}O_2$ can be considered as a high capacity cathode material (up to 200 mAh g^{-1} at C/10 rate), but slow. $LiNi_{0.33}Mn_{0.33}Co_{0.33}O_2$ can provide a lower capacity (up to 170 mAh g^{-1}), but it is a very fast electrode material, i.e., the capacity retention is more than 50% at 8C rate, while for $LiNi_{0.5}Mn_{0.5}O_2$ a 50% decrease in capacity was

already measured at 1C rate. The $LiNi_{0.4}Mn_{0.4}Co_{0.2}O_2$ electrodes demonstrate intermediate values between the above two materials in terms of both maximal capacity and rate capability. All of these materials develop a similar surface chemistry in EC–DMC/$LiPF_6$ electrolyte solutions. When using FTIR and photoelectron spectroscopies we detected polycarbonates, Li or transition metal alkyl carbonates, and perhaps alkoxides and metal fluorides, as surface species. XPS also detects surface species containing phosphorous. It is interesting that the aged $LiNi_{0.33}Mn_{0.33}Co_{0.33}O_2$ particles show, by XPS measurements, much higher Ni/M (M = Co, Mn) ratios close to the surface, compared to the bulk (pristine) ratios (which are equal to unity). This finding may reflect the pronounced reactivity of the oxygen atoms bound to Ni, and thus their reactions with acidic or electrophilic solutions species leave the Ni ions in the surface species. The above surface species passivate well all of these electrode materials in alkyl carbonate/$LiPF_6$ solutions even at elevated temperatures, which enables the impressive cycle life of cathodes comprising these materials in lithium cells.

Acknowledgment

Partial support for this work was obtained from the ISF, Israel Science Foundation.

References

[1] E. Rosen, C.D.W. Jones, J.R. Dahn, Solid State Ionics 57 (1992) 311–318; M.E. Spahr, P. Novak, B. Schnyder, O. Haas, R. Nesper, J. Electrochem. Soc. 145 (1998) 1113.
[2] J.M. Paulsen, C.L. Thomas, J.R. Dahn, J. Electrochem. Soc. 147 (2000) 861; Z. Lu, D.D. MacNeil, J.R. Dahn, Electrochem. Solid State Lett. 4 (2001) A191–A194.
[3] M.S. Islam, R.A. Davies, J.D. Gale, Chem. Mater. 15 (2003) 4280–4286.
[4] A. Manthiram, in: C. Julien, J.P. Pereira-Ramos, A. Momchilov (Eds.), New Trends in Intercalation Compounds for Energy Storage, Kluwer Academic Publisher, Netherlands, 2002, p. 157.
[5] R.V. Chebiam, F. Prado, A. Manthiram, Chem. Mater. 13 (2001) 2951–2957.
[6] Y. Arachi, H. Kobayashi, S. Emura, Y. Nakata, M. Tanaka, T. Asai, Chem. Lett. 32 (2003) 60.
[7] Y. Makimura, T. Ohzuku, J. Power Sources 119–121 (2003) 156–160.
[8] T. Ohzuku, Y. Makimura, Chem. Lett. 30 (2001) 744.
[9] T. Ohzuku, Y. Makimura, Chem. Lett. 30 (2001) 642.
[10] X. Wu, S.H. Chang, Y.H. Park, K.S. Ryu, J. Power Sources 137 (2004) 105–110.
[11] Y. Sun, Y. Xia, H. Noguchi, Electrochem, Solid State Lett. 8 (2005) A637–A640.
[12] D.-C. Li, T. Muta, L.-Q. Zhang, M. Yoshio, H. Noguchi, J. Power Sources 132 (2004) 150–155.
[13] B.J. Hwang, Y.W. Tsai, D. Carlier, G. Ceder, Chem. Mater. 15 (2003) 3676.
[14] C. Julien, M.A. Camacho-Lopez, T. Mohan, S. Chitra, P. Kalyani, S. Gopukumar, Solid State Ionics 135 (2000) 241–248.
[15] H. Kobayashi, Y. Arachi, S. Emura, H. Kageyama, K. Tatsumi, T. Kamiyama, J. Power Sources 146 (2005) 640–644.
[16] N. Mijung, Y. Lee, J. Cho, J. Electrochem. Soc. 153 (2006) A935–A940.
[17] B. Markovsky, D. Kovacheva, Y. Talyossef, M. Gorova, J. Grinblat, D. Aurbach, Electrochem. Solid-State Lett. 9 (2006) A449–A453.
[18] Y. Talyossef, B. Markovsky, R. Lavi, D. Kovacheva, G. Salitra, M. Gorova, E. Zhecheva, R. Stoyanova, D. Aurbach, J. Electrochem. Soc. 154 (2007) A682–A691.
[19] S. Gopukumar, K.Y. Chung, K.B. Kim, Electrochim. Acta 49 (2004) 803–810 (and references therein).
[20] J.N. Reimers, E. Rossen, C.D. Jones, J.R. Dahn, Solid State Ionics 61 (1993) 335.
[21] X. Luo, X. Wang, L. Lao, X. Wang, S. Gamboa, P.J. Sebastian, J. Power Sources 161 (2006) 601.
[22] E. Markevich, G. Salitra, D. Aurbach, Electrochem. Commun. 7 (2005) 1298–1304.
[23] D. Aurbach, K. Gamolsky, B. Markovsky, G. Salitra, Y. Gofer, J. Electrochem. Soc. 147 (2000) 1322–1331.
[24] B. Markovsky, Y. Talyossef, G. Salitra, D. Aurbach, H.-J. Kim, S. Choi, Electrochem. Commun. 6 (2004) 821–826.
[25] D. Aurbach, B. Markovsky, Y. Talyossef, G. Salitra, H.-J. Kim, S. Choi, J. Power Sources 162 (2006) 780–789.